Journal of Building Engineering 84 (2024) 108546

Contents lists available at ScienceDirect

Journal of Building Engineering

journal homepage: www.elsevier.com/locate/jobe

# Properties evaluation of concrete made with recycled coarse aggregate modified by graphene oxide

Qidong Wang [a], Hanbing Zhao [b,*], Zhiyu Luo [c], Shuguang Liu [d], Changshun Zhou [a], Hongxin Liu [a]

[a] Yuanpei College, Shaoxing University, Shaoxing, 312000, China
[b] School of Civil and Environmental Engineering, University of Technology Sydney, NSW, 2007, Australia
[c] Department of Civil and Environmental Engineering, National University of Singapore, 117567, Singapore
[d] School of Civil Engineering and Architecture, Wuhan University of Technology, Wuhan, 430070, China

ARTICLE INFO

*Keywords:*
Graphene oxide
Recycled aggregate concrete
Chloride ion permeability
Porosity
Micromechanical properties

ABSTRACT

Previous application of graphene oxide (GO) in recycled aggregate concrete (RAC) is the direct replacement of cement or binder to achieve performance improvement. To develop a more efficient recycled aggregate (RA) modification technique and improve the properties of the corresponding RAC, this paper performed GO solution pre-spraying and pre-soaking treatment on RA. The modification efficiency of GO was evaluated by compressive strength, interfacial transition zone (ITZ) properties, and chloride ion permeability of RAC. The results show that the pre-spraying and pre-soaking methods improved the compressive strength of RAC at different ages by 20%–28.6 % and 8.3%–30.8 %, respectively. The GO-modified RAC also exhibited lower electric flux in the chloride ion permeability tests. However, no significant effect was observed on the elastic modulus of RAC. The modified RAC showed lower total porosity and harmful pore content. Meanwhile, the GO-modified ITZ between old and new mortar had denser hydration products. As a result, the elastic modulus and hardness of the ITZ increased by 27.8%–65.8 % and 9.8%–107 %, respectively, while the width of the ITZ decreased by 15.4%–30.8 %. The good filling and nucleation effect of GO were credited with the enhancement mechanism of RA by pre-spraying and pre-soaking methods.

## 1. Introduction

The rapid development of super high-rise skyscrapers, long-span bridges, and other buildings has led to the severe exhaustion of natural resources like sand and stone. At the same time, an increasing number of older buildings are being demolished, leading to a significant amount of construction and demolition waste (C&DW). The data show that EU countries annually produce about 900 million tons of construction waste [1]. 40 % of the world's construction waste comes from China [2]. Therefore, the recycling and reusing of C&DW has become an urgent task that needs to be carried out.

Recycled aggregate concrete (RAC) is an eco-friendly construction material that serves a crucial role in protecting the environment and conserving resources. Due to the high porosity, low strength, and excessive water absorption of old mortar attached to the surface of recycled aggregate (RA) [3], the RAC normally performs worse than natural aggregate concrete (NAC) in mechanical properties and durability, which prevents the widespread application of RAC in engineering. For example, Thomase et al. [4] reported that

* Corresponding author.
*E-mail address:* Hanbing.Zhao@uts.edu.au (H. Zhao).

https://doi.org/10.1016/j.jobe.2024.108546
Received 8 November 2023; Received in revised form 6 January 2024; Accepted 12 January 2024
Available online 13 January 2024

compressive strength, splitting tensile strength and flexural strength reduced by at least 7 % when the replacement ratio of RAC was 100 %. Otsuki et al. [5] found that the interfacial transition zone (ITZ) of RAC was more porous than NAC, resulting in higher chloride penetration and carbonation depth of RAC specimens.

Currently, adding admixtures [6], optimizing preparatory design [7], removing or strengthening old mortar on RA surface [8], etc. are the most common techniques for enhancing the strength and durability of RAC. However, these modification methods usually require strict selection criteria with synergistic action of multiple polymer emulsions, and demand a large amount of time and energy [9]. For example, supplementary cementitious materials (SCM), such as fly ash (FA) and ground granulated blast furnace slag (GGBS) have become increasingly scarce in recent years and cannot meet the construction demand [10]. Mechanical abrasion [11], ultrasonic cleaning [12], acid treatment [13] on the RA surface are associated with significant energy consumption, high $CO_2$ emissions, and waste liquid contamination. Groves et al. [14] discovered that carbonation treatment can convert calcium hydroxide in old mortar into calcium carbonate and plug holes, which is contributed to improve the performance of RAC. However, carbonation has no discernible effect on RA in long-term air exposure.

In recent years, nanotechnology developed rapidly. Nanomaterials have been favored by scholars in various fields because of their good quantum size effect, macroscopic quantum tunneling effect and satisfying surface effect [15,16]. In some research [17–19], the incorporation of nano silica (NS) can improve the compressive strength of RCA to the level of NAC. Studies showed that RA can be modified by NS pre-spraying and pre-soaking methods to enhance the mechanical properties and durability of RAC [20]. Similar to NS, graphene oxide (GO) is a lamellar novel nanomaterial with good nucleation effect and 'templating' [21]. Existing research results proved that GO can promote hydration and form dense C–S–H gels in cement paste, which is contributed to improve the mechanical properties of concrete [22–24]. Moreover, GO acted as a 'bridge' between cement hydration products, which can also enhance the cohesion between phases [30]. The unique chemical structure formula of GO makes it have strong hydrophilicity and excellent dispersion property [15]. If the GO is used to modify RA, not only the pores in the old mortar can be filled, but also the microstructure of hydration products in new mortar can be changed by the nucleation effect, thus enhancing the mechanical properties and durability of RAC [15]. Devi and Khan [25,26] added 0.05 % and 0.10 % GO by weight of binder to RAC mixture. They found that 0.10 % GO improved the pore structure significantly and enhanced the compressive strength, resistance to sulfate attack and carbonation of RAC specimens [25,26]. Long et al. [27] also successfully enhanced the physico-chemical properties and microstructure of RAC by directly adding GO water solution to RAC. As introduced above, the performance of RAC could be improved in a more efficient manner by applying GO pre-spraying and pre-soaking treatment to RA. However, few people attempt and conduct comprehensively evaluations on the modification efficiency of these two approaches through micro- and macro-level tests. In addition, RAC has more complex ITZs which determine the mechanical properties and durability of concrete [28]. The attention to the micromechanical properties and porosity of ITZs in RAC prepared with GO-modified RA remains insufficient.

Therefore, this study modified RA by pre-spraying and pre-soaking methods with GO solution. The modification efficiency of these two methods was evaluated by macro-mechanical properties, micro-mechanical properties, microstructure and resistance to chloride ion penetration analysis. Finally, the modification mechanism and economic benefits of GO modification methods were discussed. This study attempts to propose a new RA modification strategy and promote the recycling of construction waste in engineering.

## 2. Materials and tests

### 2.1. Raw materials

P·O 42.5 Portland cement satisfying GB175-2007 was used in this experiment. The chemical composition of the cement is detailed in Table 1. Shenzhen Suiheng Graphene Technology Co., LTD. is responsible for GO dispersion. Table 2 lists its physical and chemical properties of GO used in this study. Fig. 1 shows particle size distribution of cement and GO with scanning electron microscopy (SEM) images. Particle size distribution and micromorphology characterized was obtained by a laser particle size analyzer (PSDA, LS230) and SEM, TM400 Plus II, respectively. It is found that GO particles are substantially smaller in size than cement particles. The cement shows large irregular clinkers and GO has a fold and sheet shape. The fine aggregate employed in this project is river sand, with a fineness modulus of 2.45. Crushing waste concrete and granite gravel between 5 and 25 cm were used as coarse aggregate in this study, named recycled aggregate (RA) and natural aggregate (NA) respectively. Apparent density, crushing index and water absorption of aggregate were tested according to BS 812, and the results are listed in Table 3. Due to the loose and porous old mortar on the surface, the apparent density, crushing index and water absorption of RA were higher than those of NA [9]. GO treatment did not significantly improve the physical properties of RA because GO is a hydrophilic material and the volume of GO coating is much lower than the volume of old mortar [29]. The modification effect of GO on RAC was mainly reflected in the promotion of cement hydration at old-new mortar interface, which will be discussed detailly in Section 3 and 4.

### 2.2. Modification process for RA

GO was used to modify RA by pre-spraying and pre-soaking methods. For pre-spraying method, 0, 0.01, 0.03 and 0.05 wt% of GO based on the mass of cement was dissolved in 200 g of deionized water and subsequently vibrated in an ultrasonic bath for 2 h to obtain

**Table 1**
Chemical compositions of cement (wt.%).

| Sample | CaO | $SiO_2$ | $Al_2O_3$ | $Fe_2O_3$ | MgO | $SO_3$ | $Na_2O$ | MnO | $K_2O$ | $P_2O_5$ | LOI |
|---|---|---|---|---|---|---|---|---|---|---|---|
| Cement | 57.8 | 20.2 | 5.2 | 8.35 | 1.89 | 2.79 | 0.13 | / | 0.82 | / | 2.82 |

**Table 2**
Basic parameters of GO.

| Layer Rate | Thickness | Flake diameter | Carbon content | Oxygen content | Dispersant | PH | Concentration |
|---|---|---|---|---|---|---|---|
| 98 % | ~1 nm | 0.5–5 μm | ~46 % | ~46 % | Water | 5~7 | 2 mg/mL |

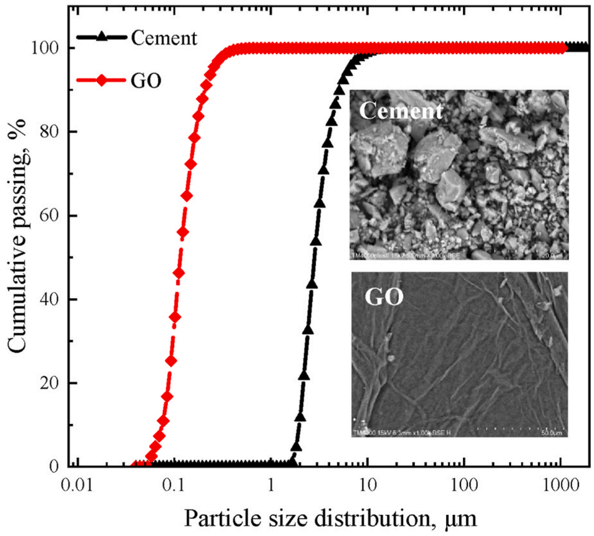


**Fig. 1.** Particle size distribution and micromorphology of cement and GO.

**Table 3**
Physical properties of coarse aggregates.

| No | Apparent density, kg/m$^3$ | Crushing index | Water absorption, % |
|---|---|---|---|
| NA | 2824 | 8.2 | 0.6 |
| Untreated RA | 2538 | 14.2 | 5.4 |
| RA treated by pre-spraying | 2539 | 14.2 | 5.2 |
| RA treated by pre-soaking | 2540 | 14.1 | 5.1 |

Note: 0.01, 0.03 and 0.05 wt% GO based on the mass of cement was used for pre-spraying treatment on RA. Due to the similarity of the physical properties of the modified RA, only the test data of RA subjected to the pre-spraying treatment with 0.05 wt% GO solution are shown in Table 3. GO solution (GO suspension: deionized water = 1:20 in volume) was used for pre-soaking treatment on RA. The detailed modification procedure is introduced in Section 2.2.

a homogeneous GO solution. RA was divided into several groups with 25 kg in each group. In order for RA surface to be uniformly sprayed with GO solution, each group of RA was poured into the mixer and sprayed with GO solution during the mixing process. Then, the pre-spraying modified RA was placed in an oven (T = 40 °C) for 7 days and marked as RA-0, RA-1, RA-3 and RA-5, respectively. The number after RA represents the concentration of GO. For example, RA-5 means the RA pre-sprayed by 0.05 wt% of GO. For pre-soaking method, GO suspension was diluted in deionized water at a volume ratio of 1:20. RA was put in the GO solution and soaked for 24 h. Finally, the pre-soaking modified RA was transported into an oven (T = 40 °C) for 7 days and labeled as RA-P.

Table 3 shows the physical characteristics of RA before and after GO modification. After pre-spraying and pre-soaking modification, the apparent density of RA increased and the water absorption reduced because nanoscale GO particles penetrated into the porous old mortar and improved the density of the RA surface. However, there was no significant change in the crushing index and water

**Table 4**
Mix proportions of RAC.

| Mixture number | w/b | Mix proportion, kg/m$^3$ | | | | | |
|---|---|---|---|---|---|---|---|
| | | Cement | Water | Sand | Coarse aggregates | Additional water | SP |
| NAC | 0.55 | 350 | 192.5 | 775 | 1161 | 6.7 | 4.5 |
| RAC-0 | 0.55 | 350 | 192.5 | 775 | 1161 | 62.7 | 4.5 |
| RAC-1 | 0.55 | 350 | 192.5 | 775 | 1161 | 60.4 | 5.6 |
| RAC-3 | 0.55 | 350 | 192.5 | 775 | 1161 | 60.4 | 6.8 |
| RAC-5 | 0.55 | 350 | 192.5 | 775 | 1161 | 60.4 | 7.9 |
| RAC-P | 0.55 | 350 | 192.5 | 775 | 1161 | 59.2 | 7.0 |

absorption of RA.

### 2.3. Mix ratio design

To investigate the properties of concrete with RA modified by GO. In this research, six group of mixtures were designed to fabricate concrete specimens with NA, RA-0, RA-1, RA-3, RA-5 and RA-P, respectively. The corresponding concrete specimens are labeled as NAC, RAC-0, RAC-1, RAC-3, RAC-5 and RAC-P, respectively. The detailed mixtures proportions are displayed in Table 4. To maintain a consistent effective water-cement ratio in each group of mixture, additional water was incorporated according to water absorption of different coarse aggregate in Table 3. The slump of each mixture is kept in the range of 120–180 mm by adjusting the content of superplasticizer (SP).

### 2.4. Test method

#### 2.4.1. Mechanical property test

In this test, two different sizes of specimens (150 mm × 150 mm × 150 mm and 150 mm × 150 mm × 300 mm) were cast for compressive strength and elastic modulus tests, respectively, according to Chinese standard GB/T 50081-2019. The loading procedure for testing elastic modulus is shown in Fig. 2. Concrete specimens cured in standard curing room for 7, 28 and 90 days were removed and used for mechanical property tests. Each group of tests was repeated three times.

#### 2.4.2. Chloride ion permeability test

Chloride permeability test steps are based on Chinese standard GB/T 50082-2009. The Φ100mm × 50 mm cylindrical concrete specimens with a 28-day curing age were placed in an oven at 40 °C for 48 h. The lateral surface of specimens was then covered with a layer of epoxy resin and vacuum saturated. In the test tank, the positive pole of the specimen was injected with NaOH solution at a concentration of 0.3 mol/L. Correspondingly, the negative pole was injected with 3 % NaCl solution. A DC voltage of 60 V was applied in the axial direction. The current passing through the specimen was recorded once every 5 min, and the total flux for a duration of 6 h was calculated. The chloride ion penetration test for each group of specimens was repeated three times.

#### 2.4.3. Microstructure analysis

RA with and without GO modification was impregnated in isopropyl alcohol to terminate hydration in old mortar. After drying in an oven (40 °C) for 48 h, samples were coated with a layer of 5 nm gold. SEM, JSM-6360LV was used to observe micromorphology of RA modified by GO. In addition, the cement paste near modified RA was broken down into small fragments and the pore size distribution was characterized by a mercury intrusion porosimetry (MIP, MAC Autopore 950). Different from SEM tests, samples for MIP tests were immersed in ethanol for 7 days to stop further hydration and then dried in a vacuum oven at 60 °C for 3 days to eliminate any residual ethanol. One sample for each group was prepared for MIP tests.

#### 2.4.4. Nanoindentation test

Hysitron TiPremier nano-indenter (Bruker Company, USA) equipped with a Berkovich tip was used to characterize micro-mechanical properties of GO modified ITZs in RAC. A concrete specimen was cut into a cubic sample with the side length of 10 mm, and then, the sample was impregnated by epoxy resin under vacuum condition. After the epoxy resin solidified, the observing surface of the sample was ground by 300, 600, 800 and 1200 grit abrasive papers for 15 min each, followed by 0.3 μm and 0.05 μm alumina slurry polishing for 30 min each. The residual impurities on the sample surface were removed by ultrasonic cleaner.

In the selected matrix region, the tip was pressed into cement paste until the normal load reaching 4 mN. The normal load maintained at the maximum value for 2 s and then the unloading process finished in 5 s. The corresponding normal load ($p$) -displacement ($h$) curve was obtained (see Fig. 3). The elastic modulus and hardness of test regions can be calculated according to the $p$-$h$ curves. Based on Hertz theory [30], it is assumed that the surface of the material is clean and smooth. The indentation depth is far less than the geometric size of the material, thus the relationship between normal load and indentation depth is obtained:

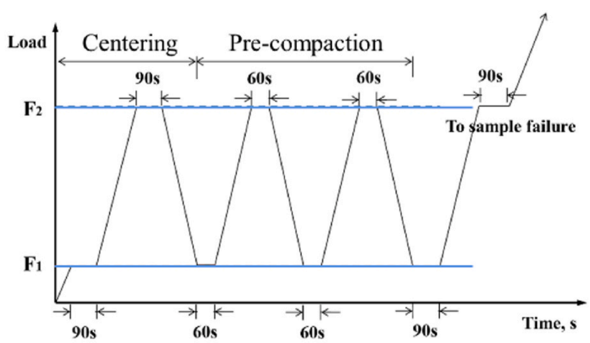


**Fig. 2.** Loading procedure of concrete elastic modulus test. ($F_1$ represents the load value at 0.5 MPa; $F_2$ represents the load value corresponding to the axial compressive strength of 1/3).

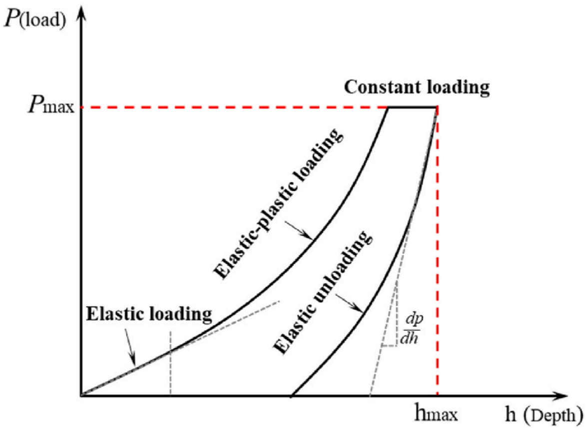


**Fig. 3.** Typical load-displacement curve of nanoindentation.

$$S = \frac{dp}{dh} = \frac{2}{\sqrt{\pi}} E_r \sqrt{A} \tag{1}$$

where, $h$ is the indentation depth; $p$ is the normal load; S is the contact stiffness; $A$ stands for the contact area; $E_r$ is the reduced elastic modulus determined by descending part of the $p$-$h$ curve. The following equation shows the relationship between $E_r$ and the elastic modulus $E$ of the cementitious materials:

$$E = (1 - \nu^2) \times \left[\frac{1}{E_r} - \frac{(1 - \nu_i^2)}{E_i}\right]^{-1} \tag{2}$$

where, $\nu$ is the Poisson's ratio of materials, which was set as 0.24 in this study; $E_i$ and $\nu_i$ are the elastic modulus and Poisson's ratio of the tip respectively. For the Berkovich tip used in this study, $E_i$ and $\nu_i$ are 1140 GPa and 0.07 respectively.

Grid nanoindentation tests were performed on ITZ between aggregate and old mortar (ITZ-I), and between old mortar and new mortar (ITZ-II), respectively. For each ITZ, 4 × 25 grid nanoindentation tests were conducted at a randomly selected region. The horizontal and vertical spacing between the two indentation points is 5 μm, as exhibited in Fig. 4.

## 3. Results

### 3.1. Mechanical properties

Fig. 5 (a) shows the compressive strength of RAC at various ages. It can be observed that the compressive strength of concrete specimens reduced dramatically when NA was substituted by RA. The compressive strength growth rate compared to RAC-0 is shown in Fig. 5 (b). NAC specimens at 7 d, 28 d and 90 d were 33.3 %, 32.9 % and 30.4 % respectively higher than RAC-0 in compressive strength. The reason is that the porous old mortar attached to the surface of RA weakened the bonding performance with new paste matrix [15]. In addition, the compactness of RAC was lower than NAC because of low apparent density of RA (see Table 3). As a result, the compressive strength of concrete specimens made with RA reduced. However, the compressive strength of RAC-P increased by 20%–28.6 % compared to RAC-0 at different ages. For RA modified by GO pre-spraying method, the compressive strength of specimens at various ages was significantly improved, especially at the early age. Compared with RAC-0, the compressive strength of RAC-1,

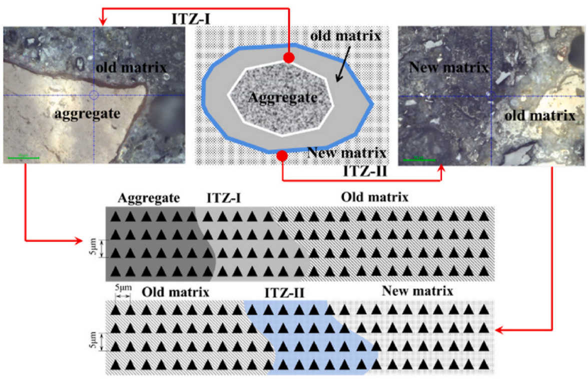


**Fig. 4.** Schematic of the grid nanoindentation area.

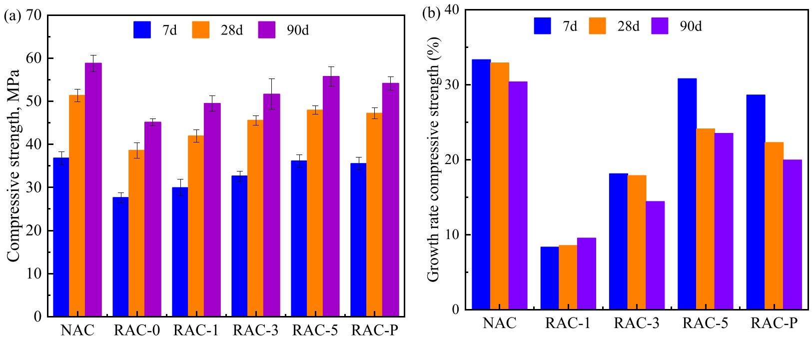


**Fig. 5.** (a) Compressive strength and (b) growth rate of compressive strength at various ages.

RAC-3 and RAC-5 increased by 8.3 %, 18.1 % and 30.8 % at 7 days, and 9.5 %, 14.4 % and 23.5 % at 90 days, respectively. When using the pre-spraying method, it was observed that the modification efficiency on RA increased gradually with higher GO concentrations. It is worth noting that the compressive strength of RAC-5 was very close to NAC at various ages and showed higher compressive strength compared with RAC-P.

The elastic modulus and increasing ratio relative to RAC-0 are shown in Fig. 6 (a) and (b) respectively. When NA was replaced by RA without any modification, the elastic modulus of specimens decreased by 13.7 %–14.6 % at different ages. The modifying results in elastic modulus were not as prominent as the results in compressive strength. Compared with RAC-0, the elastic modulus of RAC-P, RAC-1, RAC-3 and RAC-5 increased by 6.6 %–7.1 %, 1.8 %–3.8 %, 3.9 %–6.8 % and 7 %–9.1 %, respectively at different ages, which agrees with the findings of previous researches [31,32].

### 3.2. *Chloride ion permeability*

Chloride ion permeability is one of the crucial metrics for assessing RAC durability. The electric flux of RAC is shown in Fig. 7. High electric flux represents a poor resistance to chloride ion penetration. It can be found that among all samples, NAC exhibited the lowest electric flux, while RAC-0 showed the highest electric flux. GO modification can effectively reduce the electric flux of RAC in chloride ion permeability tests. As compared to RAC-0, the electric flux of RAC-P, RAC-1, RAC-3, and RAC-5 decreased by 13.5 %, 9.9 %, 11.7 % and 15.2 %, respectively. To summarize, pre-spraying and pre-soaking treatment can effectively improve the resistance to chloride ion permeability of RAC, which is mainly attributed to the refinement of GO on the pore structure of RAC. Regarding the modification techniques in this study, the pre-spray modification therapy is marginally superior to the pre-soaking modification treatment.

### 3.3. *Microstructure of aggregate-paste matrix interface*

Fig. 8 shows the microstructure of RA before and after GO modification. It is readily discernible that C–S–H gel, CH, Aft, micro-cracks and pores are mainly distributed around the aggregate. In Fig. 8 (a), hydration products were relatively loose and disorderly, with more CH crystals, which is consistent with previous research results [15]. After GO pre-spraying modification, the dispersive C–S–H gels were connected together and a dense microstructure emerged. Similarly, the microstructure near RA was also improved after GO pre-soaking treatment on RA. According to Powwes-Brunauer model [33], C–S–H gel has a propensity to cluster because of its layered structure, large specific surface area, and strong adhesion. GO also has a huge specific surface area, and its adsorption can largely promote C–S–H agglomeration [34,35]. Meanwhile, functional groups containing oxygen on GO surface can provide hydration reaction sites to induce and regulate the content, crystal morphology and aggregation state of hydration products [36].

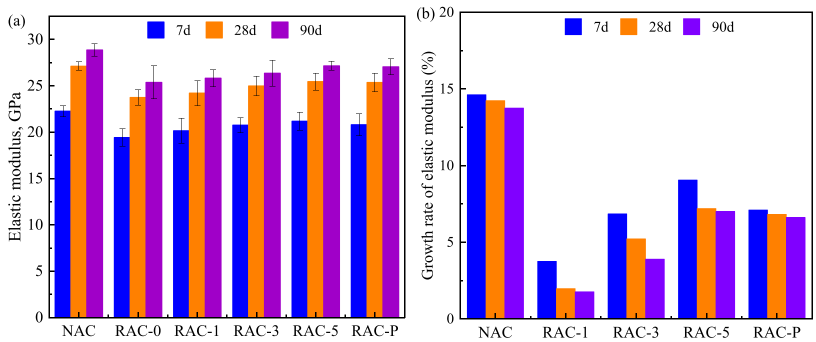


**Fig. 6.** (a) Elastic modulus and (b) growth rate of elastic modulus at various ages.

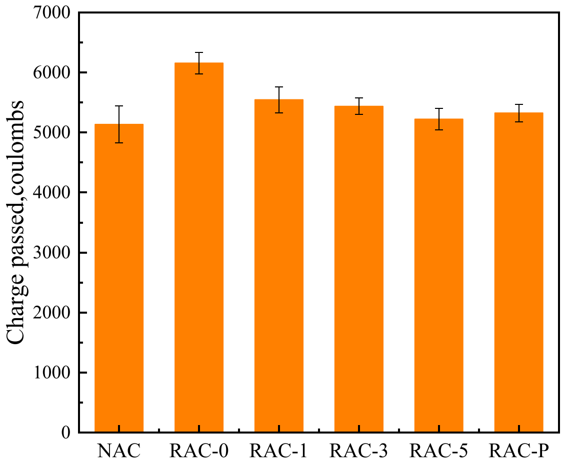


**Fig. 7.** Chloride penetration resistance of RAC.

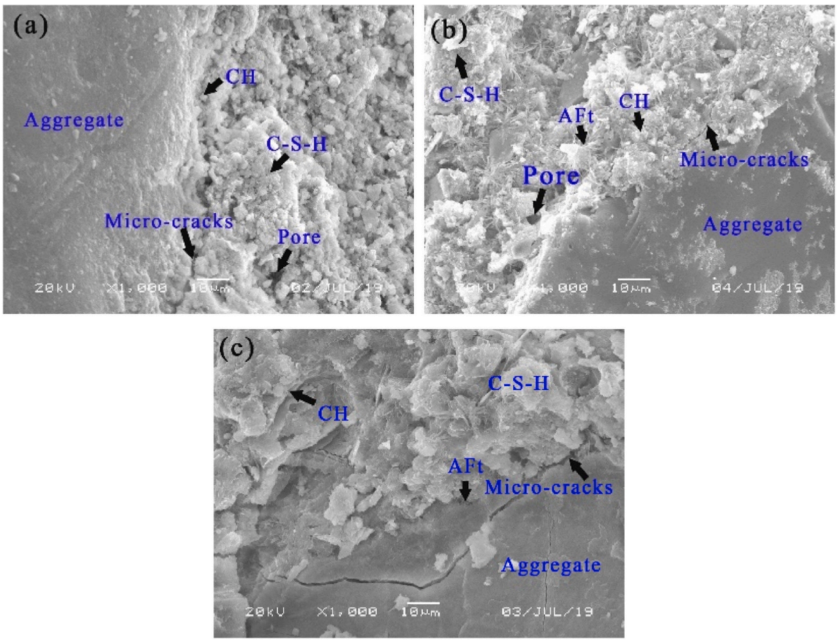


**Fig. 8.** Microstructure of RA before and after GO modification: (a) RAC-0, (b) RAC-5, and (c) RAC-P.

### 3.4. *Pore structure*

Pores in cement-based materials are usually divided into four categories based on equivalent diameter namely innocuous pore with a size less than 20 nm, less harmful pore with a size between 20 and 50 nm, harmful pore with a size between 50 and 200 nm, and more harmful pore with a size greater than 200 nm [6,37]. Fig. 9 shows the cumulative porosity of NAC and RAC at 28 days and the proportion of pores with different sizes. As can be seen from Fig. 9 (a), NAC had the lowest porosity of 13.11 %, while RAC-0 had the highest porosity of 20.45 %. However, when NA was replaced by RA modified by GO, the porosity of the sample decreased significantly. Compared with RAC-0, the total porosity of RAC-5 and RAC-P decreased by 27.8 % and 21.4 %, respectively. It has been reported that pores with equivalent diameter larger than 50 nm have unfavorable effects on the mechanical properties of concrete [37–40]. In Fig. 9 (b), the proportion of harmful and more harmful pores in NAC was only 4.11 %, while the corresponding proportion in RAC-0 was up to 14.8 %. The detrimental pores in RAC-5 and RAC-P with an equivalent diameter larger than 50 nm was reduced by 35.5 % and 27.5 %, respectively, compared to RAC-0. Therefore, it can be concluded that the pore structure of RAC can be improved by GO modification on RA surface [41,42]. This refinement of the pore structure explained the enhancement of the mechanical properties and the resistance to chloride ion permeation of the RAC.

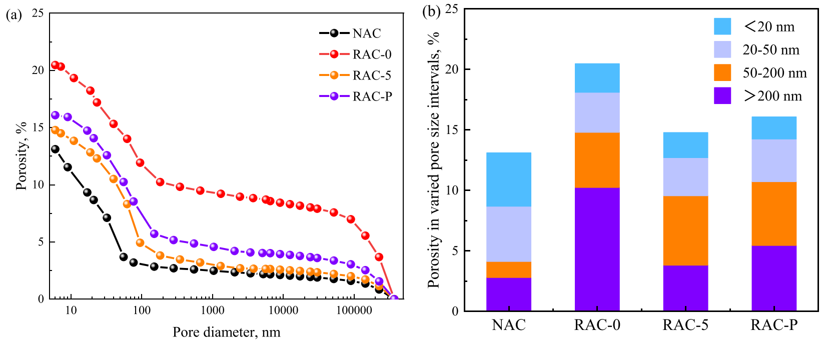


**Fig. 9.** Impact of GO on pore structure of RAC: (a) Cumulative porosity, and (b) Proportion of pores different sizes.

### 3.5. Nanoindentation

RAC is an inhomogeneous composite material. In addition to the cement paste, many researchers are keen to study the bonding properties of ITZs, which are regarded as the weakest region in concrete. In this paper, nanoindentation tests were conducted on ITZs in RAC-0, RAC-5 and RAC-P to evaluate the modification results of GO treatments. The main characteristics obtained in nanoindentation tests include elastic modulus, hardness and thickness of ITZ-I and ITZ-II in RAC. The test results are shown in Table 5.

Fig. 10 shows contour maps of elastic modulus of ITZ-I in RAC before GO treatment. The dark blue regions represent relatively weak areas. The pink and green areas have higher elastic modulus, usually representing aggregates, high-density C–S–H gels, unhydrated cement particles and CH crystals. By observing the color variation trend in Fig. 10, it can be clearly seen that the dark blue area is mainly distributed between the aggregate and old mortar matrix. This feature serves as an important indicator of ITZ-I in RAC, which can be used to evaluate the overall strength and durability of the concrete material.

It is reported that the ITZ thickness can be determined based on the elastic modulus variation with the distance from the aggregate boundary [43]. The thickness of ITZ can be seen as an indicator to evaluate the mechanical properties and durability of RAC [44]. The quantified elastic modulus and hardness distribution of ITZ-I in RAC sample with and without GO treatment are displayed in Fig. 11. It is discovered that the elastic modulus at the ITZ-I was the lowest, compared with aggregate and matrix. The average elastic modulus of the ITZ-I in different samples ranged from 14.5 to 15.4 GPa, and the thickness of ITZ-I was about 45 μm. Compared with RAC-0, both RAC-5 and RAC-P showed slightly higher average elastic modulus and hardness in the ITZ-I region. Specifically, the average elastic modulus of the ITZ-I in RAC-5 and RAC-P increased by 5.2 % and 1.3 %, respectively, and the hardness is increased by 18.3 % and 11.7 %, respectively. It is concluded that GO modification on ITZ-I is difficult to be detected by nanoindentation tests, mainly because GO solution cannot easily penetrate through microcracks in old mortar to reach the aggregate surface and produce effects, which is similar to previous research results [6].

Fig. 12 exhibits contour maps of the elastic modulus distribution of ITZ-II in RAC. Dark blue areas are low elastic modulus regions, while green and pink parts are regions with higher elastic modulus. From left to right, the nanoindentation grid started at the old mortar and ended at the new mortar matrix. It can be found that there were more blue areas distributed between the new and old mortar matrix, which indicates a poorer cohesion between these two regions.

Fig. 13 shows the elastic modulus and hardness of ITZ-II in RAC with and without GO treatment. It is evident that the elastic modulus of the old mortar (left of ITZ-II) in different samples was significantly higher than the elastic modulus of the new mortar (right of ITZ-II), and the former had an obvious discreteness. This can be explained by more complicated phases and a greater difference in the hydration degree in the old mortar. In Fig. 13 (a), the thickness of ITZ-II in RAC-0 was around 65 μm, and the average elastic modulus and hardness were 11.89 GPa and 0.41 GPa, respectively. After GO pre-spraying modification on RA, the elastic modulus and hardness of ITZ-II improved with a narrow thickness. Compared with RAC-0, the thickness of ITZ-II in RAC-5 decreased by 30.8 %. Correspondingly, the average elastic modulus and hardness improved by 65.8 % and 107 %, respectively. Similar to RAC-5, after GO

**Table 5**
Thickness and micromechanical properties of GO-modified ITZs in RAC.

| Group | | RAC-0 | RAC-5 | RAC-P |
|---|---|---|---|---|
| ITZ-I | Thickness (μm) | 45 | 45 | 45 |
| | Mean modulus (GPa) | 15.4 | 16.2 | 15.6 |
| | Mean hardness (GPa) | 0.6 | 0.71 | 0.67 |
| ITZ-II | Thickness (μm) | 65 | 45 | 55 |
| | Mean modulus (GPa) | 11.89 | 19.72 | 15.2 |
| | Mean hardness (GPa) | 0.41 | 0.85 | 0.45 |
| New matrix (ITZ-II) | Mean modulus (GPa) | 19.67 | 24.73 | 23.7 |
| | Mean hardness (GPa) | 0.71 | 1.19 | 0.76 |
| Old matrix (ITZ-II) | Mean modulus (GPa) | 33.95 | 31.9 | 30 |
| | Mean hardness (GPa) | 1.31 | 0.75 | 1.29 |

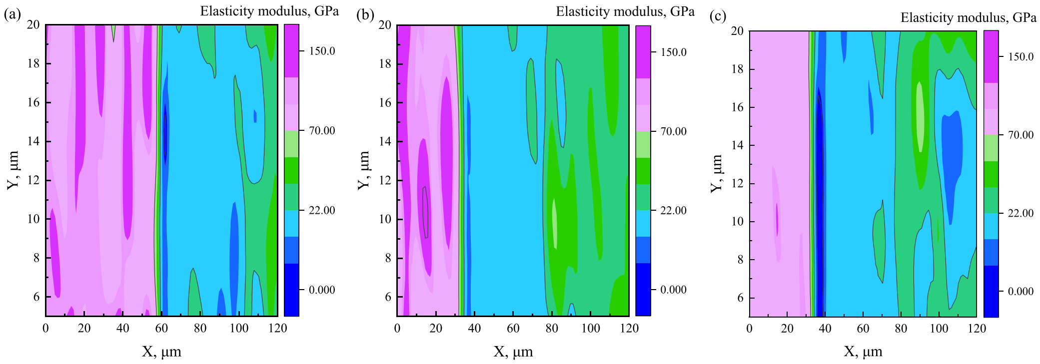


**Fig. 10.** The contour maps of the elastic modulus distribution in the ITZ-I of RAC at 28 days: (a) RAC-0, (b) RAC-5, (C) RAC-P.

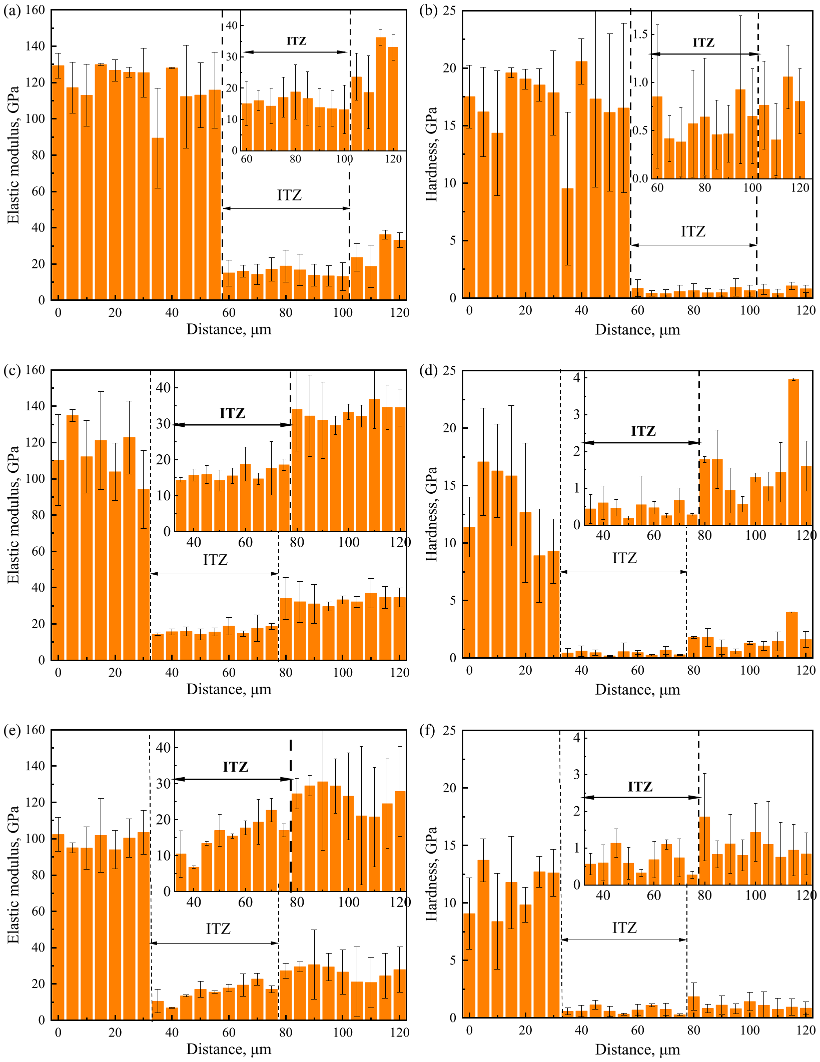


**Fig. 11.** Elastic modulus and hardness distribution of ITZ-I in RAC: (a) and (b) RAC-0, (c) and (d) RAC-5, (e) and (f) RAC-P.

pre-soaking modification on RA, the micromechanical properties of ITZ-II in RAC were also improved. Compared with RAC-0, the thickness of ITZ-II in RAC-P reduced by 15.4 %, while the average elastic modulus and hardness increased by 27.8 % and 9.8 %, respectively. In conclusion, GO modification can effectively enhance the bonding performance of ITZ-II in RAC, and the enhancement

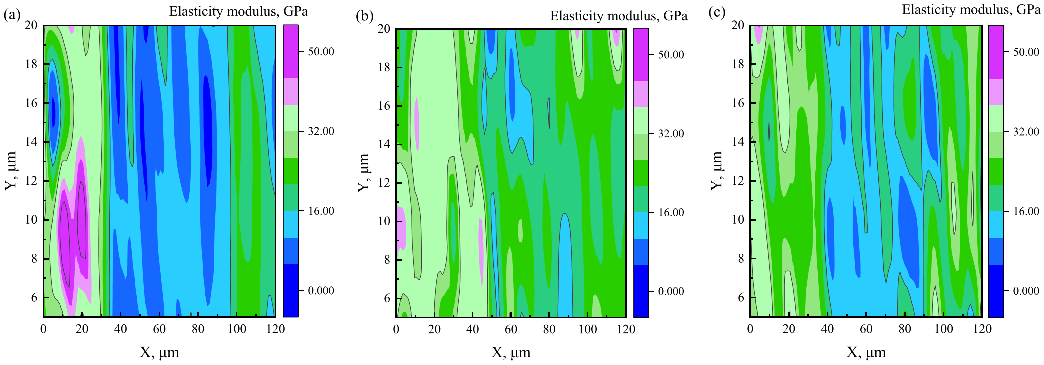


**Fig. 12.** The contour maps of elastic modulus distribution in the ITZ-II of RAC at 28 days: (a) RAC-0, (b) RAC-5, (c) RAC-P.

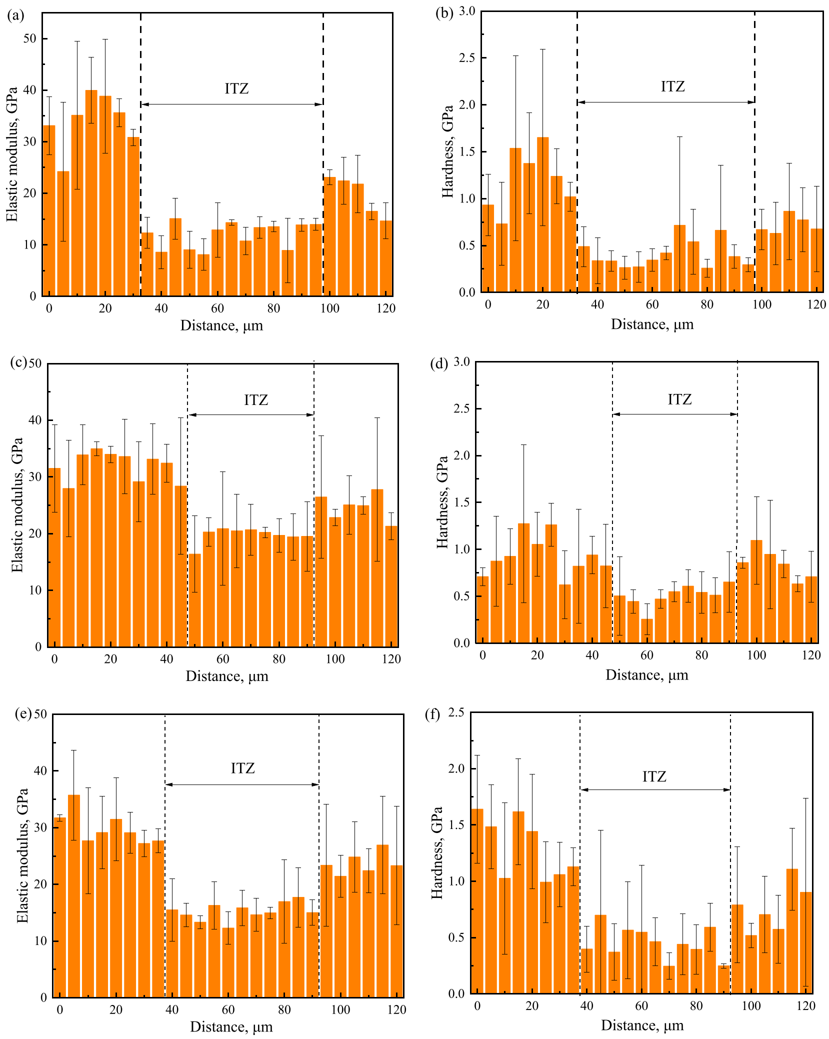


**Fig. 13.** Elastic modulus and hardness distribution in ITZ-II of RAC: (a) and (b) RAC-0, (c) and (d) RAC-5, (e) and (f) RAC-P.

efficiency of pre-spraying method was better than that of pre-soaking method.

## 4. Discussion

### 4.1. Modification mechanism of GO solution

The mechanical properties and resistance to chloride ion permeability of concrete specimens reduced significantly when NA was replaced by RA. Interestingly, GO pre-spraying and pre-soaking treatments on RA brought an improvement in mechanical properties (see Figs. 5 and 6) and resistance to chloride ion permeability (Fig. 7) of concrete specimens, especially in compressive strength at early age (see Fig. 5). In terms of enhancement efficiency, pre-spraying method is slightly superior to pre-soaking method. The modification mechanism of GO solution on RAC performance can be understood from both physical and chemical perspectives [45]. The mechanism of GO action in the ITZ of the RAC is illustrated in Fig. 14.

(1) Filling effect: GO particles can fill pores and microcracks in the old mortar attached to the surface of RA. The average size of GO particle was 115 nm (see Fig. 1). There were a large volume of pores and cracks with equivalent diameter larger than 100 nm (see Fig. 9), which can be filled by GO particles because of its good filling effect [46]. GO can also penetrate into interfaces between C–S–H gels individually or collectively to make up for the defects in ITZs between old and new mortar [47,48], making the microstructure of the RAC matrix denser. With regard to the pore size distribution (see Fig. 9), the total porosity in RAC decreased by 21.4%–27.8 % after GO pre-spraying and pre-soaking modification. Moreover, the proportion of harmful pores (pore size > 50 nm) in RAC-5 and RAC-P decreased by 27.5%–35.5 % compared to RAC-0, which further confirmed that RA modified by GO had a better microstructure. This explains why RAC-5 and RAC-P showed higher compressive strength and better resistance to chloride ion permeability.

(2) Nucleus effect: GO adsorbed on the surface of the old mortar will accelerate cement hydration of the new mortar and generate more C–S–H gel, thus strengthening the cohesion properties of ITZs. This can be confirmed by SEM images (see Fig. 8) and nanoindentation test results (see Figs. 10–13). Some researchers pointed out that during the cement hydration process, the concentrations of $Ca^{2+}$, $SiO_4^{4-}$ and $SO_4^{2-}$ ions in pore solution increased rapidly, and stable crystal nuclei began to form after reaching the critical nucleation concentration [19]. However, the GO adsorbed on the surface of the old mortar provided "prefabricated" nuclei for the hydration process. The production of hydration products was no longer restricted by the critical nucleation concentration. Although the ion concentration was lower than the required threshold, the hydration products can develop on the GO surface to form the C–S–H phase, thus accelerating the hydration reaction rate [45,46]. Loose C–S–H can be deposited on the surface of the flake GO, and a dense and uniform microstructure was gradually formed in the network structure of GO [49].

Table 6 summarizes the effects of existing modification methods on RAC compressive strength at 28 days. Compared with other methods, the GO solution pre-spraying and pre-soaking treatment of RA proposed in this work can significantly enhance the compressive strength of RAC, which offers a fresh concept to better utilize construction waste.

In addition, the enhancing effect of pre-spraying and pre-soaking treatment of RA with GO solution on elastic modulus was not as obvious as that on compressive strength. This is because most of GO solution remained at the surface of the old mortar and only a small portion of GO was able to penetrate through microcracks and reach the surface of aggregate. As a result, the GO-reinforced matrix accounted for only a small portion of the total matrix in RAC. This was confirmed by the results in nanoindentation tests (see Table 5). Based on previous research [29], the elastic modulus of concrete can be estimated via the following equation:

Series

$$\text{Model}: \frac{1}{E} = \sum_{i=1}^{n} \frac{V_i}{E_i} \tag{3}$$

Parallel

$$\text{Model}: E = \sum_{i=1}^{n} E_i \bullet V_i \tag{4}$$

where $E_i$ and $V_i$ are the elastic modulus and volume fraction of different materials in concrete respectively; $n$ is the total number of type of phases in concrete. The elastic modulus is determined by the micromechanical properties of the phases in concrete. However,

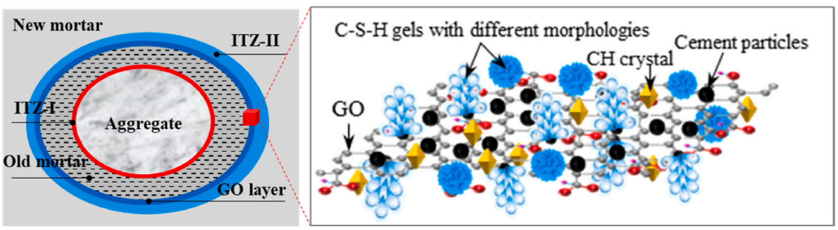


**Fig. 14.** Schematic diagram of ITZ enhancement by GO.

**Table 6**
The impact of various modification methods on the compressive strengths of RAC at 28 days.

| Modification approach | RA content (%) | w/b | Testing conditions | Variation of compressive strength (%) | Refs. |
|---|---|---|---|---|---|
| Pozzolanic materials | 100 | 0.4 | Adding 50 % blast furnace slag | 12 | [50] |
| | 100 | 0.44 | Adding 10 % FA and 10 % SF | 9.2 | [51] |
| Optimize the mixing process | 5–30 | 0.45 | Two-stage mixing approach | 0.02–10.7 | [7] |
| Acid treatment | 5–30 | 0.45 | Pre-soaking of RA in HCl, $H_2SO_4$, $H_3PO_4$ solution | 0.07–14 | [52] |
| Mechanical abrasion | 10–40 | 0.38 | Mechanical grinding for 5 min | 3.8–20.8 | [53] |
| Carbonation technique | 0–100 | 0.28 | Gas pressure of 0.1 Bar or 5.0 Bar for 24 h | 0.6–22.6 | [54] |
| Biodeposition | 100 | 0.35 | Pre-soaking of RA in bacterial culture solution | 20.9 | [55] |
| Modification of nanomaterials | 100 | 0.4 | 3 % NS | 18 | [20] |
| | 50 | 0.4 | 1 % and 2 % NS | 9–23 | [56] |
| | 100 | 0.3 | Adding 0.025 %–0.075 % GO | 8.2–16.8 | [57] |
| | 100 | 0.4 | Pre-soaking of RA in 2 % NS solution | 25 | [24] |
| | 100 | 0.55,0.56 | Pre-spraying of RA in 1–8 % NS solution | 3.2–11.2 | [58] |
| | 100 | 0.55 | Pre-soaking of RA in GO solution | 22.3 | This work |
| | | | Pre-spraying of RA in GO solution | 8.5–24.1 | |

there is less enhanced matrix in RAC after pre-spraying and pre-soaking treatment with GO solution of RA. As a result, the change in the elastic modulus of RAC was not obvious.

### 4.2. Economic benefits of GO modification

The economic benefits of different RACs are evaluated by calculating the cost of paste per cubic meter ($C_p$, \$/MPa·m$^3$), as shown in Eq. (3) [6].

$$C_p = \text{Cost} / f_c \tag{5}$$

Where, $f_c$ (MPa) is the compressive strength of concrete specimens at 28 d. The costs of raw materials reported in previous research are presented in Table 7.

To more comprehensively evaluate the GO modification on RA, this paper conducted an economic analysis to show the feasibility of using GO-modified RA in engineering. Fig. 15 shows the cost of concrete preparation in this study. According to the calculation results, concrete costs are slightly lower than NAC when a small amount of GO solution was used, and the $C_p$ value is close to RAC-0. As GO content increases, the cost of concrete gradually increases, mainly due to the expensive GO itself. It is worth noting that the compressive strength of RAC was close to that of NAC when the appropriate amount of GO was used in pre-spraying treatment, which is conducive to applying RAC in engineering. In addition, the cost of pre-soaking treatment designed in this study is close to pre-spraying method with 0.03 wt% of GO solution. With the gradual maturation of GO preparation technology, its cost will decrease, which will be more meaningful for the application of GO in RAC.

## 5. Conclusion

In this study, 0.01, 0.03 and 0.05 wt% GO based on the mass of cement was used to pre-spraying treatment on RA. GO solution with a volume ratio of GO to deionized water of 1:20 was used to pre-soaking treatment on RA. According to the compressive strength, chloride ion permeability, microscopic properties and financial benefits of GO modified RAC obtained in this study, the following conclusions can be drawn:

The compressive strength of the RAC improved significantly after GO solution pre-spraying and pre-soaking treatment of RA, especially at the early stage. At different ages, the compressive strength of RAC modified by pre-soaking method increased by 20%–28.6 % compared to RAC-0. The modification performance of pre-spraying method on compressive strength is highly related to the concentration of GO solution. When the concentration of GO solution was 0.01 wt%, the compressive strength improving ratio at 7 days, 28 days and 90 days was 8.3 %, 8.7 % and 9.5 % respectively. However, for 0.05 wt% of GO solution in pre-spraying method, the compressive strength improving ratio at different ages was 30.8 %, 24.7 % and 23.5 % respectively, compared to RAC-0. In contrast, the elastic modulus of RAC was not significantly affected by pre-spraying and pre-soaking treatment. In addition, chloride ion

**Table 7**
Cost of the raw materials in this study.

| Types of mixture | Cost for one ton (\$) | References |
|---|---|---|
| Cement | 77.5 | [59] |
| NCA | 18.6 | [59] |
| RCA | 2.325 | [59] |
| Sand | 27.9 | [60] |
| PS | 5245 | [6] |
| GO | 286825 | This work |

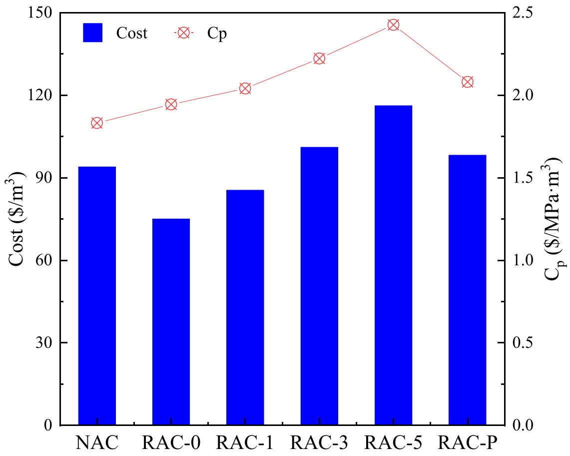


**Fig. 15.** Economic benefit analysis of GO modification.

permeability tests show that the RAC modified by GO pre-spraying and pre-soaking method achieved a lower electric flux.

According to microscopic results, after the pre-spraying and pre-soaking treatment of RA with GO solution, the hydration products close to the aggregates became denser. The total porosity and the number of harmful pores (the pore size larger than 50 nm) in the samples with GO modified RA were dramatically reduced. The nanoindentation results show that the elastic modulus and hardness of ITZ-II in the GO modified RAC increased by 27.8 %–65.8 % and 9.8 %–107 %, respectively. Meanwhile, the width of ITZ-II decreased by 15.4%–30.8 %. However, GO had no significant effect on micromechanical properties of old mortar and ITZ-I in RAC. The enhancement mechanism of GO was mainly credited to the good filling effect and the nucleation effect, resulting in a denser ITZ.

Since GO is currently expensive in the market, using GO solution to pretreat RA will increase the cost of RAC. The cost of the GO solution pre-soaking used in this study is similar to that of 0.03 wt% GO pre-spraying treatment. With the development of GO preparation technology in the future, the cost of this modification scheme will be greatly reduced and the application of RAC in construction will also be promoted.

## CRediT authorship contribution statement

**Qidong Wang:** Investigation, Writing – original draft, Writing – review & editing. **Hanbing Zhao:** Conceptualization, Methodology, Writing – review & editing. **Zhiyu Luo:** Writing – review & editing. **Shuguang Liu:** Writing – review & editing. **Changshun Zhou:** Investigation. **Hongxin Liu:** Investigation.

## Declaration of competing interest

The authors declare no conflicts of interest.

## Data availability

Data will be made available on request.

## Acknowledgements

This work was financially supported by the National Natural Science Foundation of Zhejiang province (Grant No. LHY22E080001).

## References

[1] J. Staunton, C.D. Williams, L. Morrison, T. Henry, G.T.A. Fleming, M.J. Gormally, Spatio-temporal distribution of construction and demolition (C&D) waste disposal on wetlands: a case study, Land Use Pol. 49 (2015) 43–52.
[2] H. Yang, J. Xia, J.R. Thompson, R.J. Flower, Urban construction and demolition waste and landfill failure in Shenzhen, China, Waste Manag. 63 (2017) 393–396.
[3] M. Bravo, J. de Brito, J. Pontes, L. Evangelista, Durability performance of concrete with recycled aggregates from construction and demolition waste plants, Construct. Build. Mater. 77 (2015) 357–369.
[4] J. Thomas, N.N. Thaickavil, P.M. Wilson, Strength and durability of concrete containing recycled concrete aggregates, J. Build. Eng. 19 (2018) 349–365.
[5] N. Otsuki, S.-i. Miyazato, W. Yodsudjai, Influence of recycled aggregate on interfacial transition zone, strength, chloride penetration and carbonation of concrete, J. Mater. Civ. Eng. 15 (5) (2003) 443–451.
[6] P. Zhan, X. Zhang, Z. He, J. Shi, O. Gencel, N.T. Hai Yen, G. Wang, Strength, microstructure and nanomechanical properties of recycled aggregate concrete containing waste glass powder and steel slag powder, J. Clean. Prod. 341 (2022) 130892.
[7] V.W.Y. Tam, C.M. Tam, Diversifying two-stage mixing approach (TSMA) for recycled aggregate concrete: TSMAs and TSMAsc, Construct. Build. Mater. 22 (10) (2008) 2068–2077.

[8] X. Wang, J. Xu, Z. Wang, W. Yao, Use of recycled concrete aggregates as carriers for self-healing of concrete cracks by bacteria with high urease activity, Construct. Build. Mater. 337 (2022) 127581.
[9] J. Liu, K. Ma, J. Shen, J. Zhu, G. Long, Y. Xie, B. Liu, Influence of recycled concrete aggregate enhancement methods on the change of microstructure of ITZs in recycled aggregate concrete, Construct. Build. Mater. 371 (2023) 130772.
[10] N. Arabi, H. Meftah, H. Amara, O. Kebaïli, L. Berredjem, Valorization of recycled materials in development of self-compacting concrete: mixing recycled concrete aggregates – windshield waste glass aggregates, Construct. Build. Mater. 209 (2019) 364–376.
[11] H.K.A. Al-Bayati, P.K. Das, S.L. Tighe, H. Baaj, Evaluation of various treatment methods for enhancing the physical and morphological properties of coarse recycled concrete aggregate, Construct. Build. Mater. 112 (2016) 284–298.
[12] M. Pepe, R.D. Toledo Filho, E.A.B. Koenders, E. Martinelli, Alternative processing procedures for recycled aggregates in structural concrete, Construct. Build. Mater. 69 (2014) 124–132.
[13] H. Katkhuda, N. Shatarat, Improving the mechanical properties of recycled concrete aggregate using chopped basalt fibers and acid treatment, Construct. Build. Mater. 140 (2017) 328–335.
[14] G.W. Groves, A. Brough, I.G. Richardson, C.M. Dobson, Progressive changes in the structure of hardened C3S cement pastes due to carbonation, J. Am. Ceram. Soc. 74 (11) (1991) 2891–2896.
[15] P. Zhan, J. Xu, J. Wang, J. Zuo, Z. He, A review of recycled aggregate concrete modified by nanosilica and graphene oxide: materials, performances and mechanism, J. Clean. Prod. 375 (2022) 134116.
[16] P. Zhan, Z. He, Z. Ma, C. Liang, X. Zhang, A.A. Abreham, J. Shi, Utilization of nano-metakaolin in concrete: a review, J. Build. Eng. 30 (2020) 101259.
[17] B.B. Mukharjee, S.V. Barai, Mechanical and microstructural characterization of recycled aggregate concrete containing silica nanoparticles, J. Sustain. Cem.-Based Mater. 6 (1) (2017) 37–53.
[18] S. Erdem, S. Hanbay, Z. Guler, Micromechanical damage analysis and engineering performance of concrete with colloidal nano-silica and demolished concrete aggregates, Construct. Build. Mater. 171 (2018) 634–642.
[19] W. Li, Z. Luo, C. Long, C. Wu, W.H. Duan, S.P. Shah, Effects of nanoparticle on the dynamic behaviors of recycled aggregate concrete under impact loading, Mater. Des. 112 (2016) 58–66.
[20] B.B. Mukharjee, S.V. Barai, Influence of Nano-Silica on the properties of recycled aggregate concrete, Construct. Build. Mater. 55 (2014) 29–37.
[21] I.H. Alvi, Q. Li, Y. Hou, C.C. Onyekwena, M. Zhang, A. Ghaffar, A critical review of cement composites containing recycled aggregates with graphene oxide nanomaterials, J. Build. Eng. 69 (2023) 105989.
[22] H. Peng, Y. Ge, C.S. Cai, Y. Zhang, Z. Liu, Mechanical properties and microstructure of graphene oxide cement-based composites, Construct. Build. Mater. 194 (2019) 102–109.
[23] B.B. Mukharjee, S.V. Barai, Development of construction materials using nano-silica and aggregates recycled from construction and demolition waste, Waste Manag. Res. 33 (6) (2015) 515–523.
[24] F. Shaikh, V. Chavda, N. Minhaj, H.S. Arel, Effect of mixing methods of nano silica on properties of recycled aggregate concrete, Struct. Concr. 19 (2) (2018) 387–399.
[25] S.C. Devi, R.A. Khan, Effect of sulfate attack and carbonation in graphene oxide–reinforced concrete containing recycled concrete aggregate, J. Mater. Civ. Eng. 32 (11) (2020) 04020339.
[26] S.C. Devi, R.A. Khan, Compressive strength and durability behavior of graphene oxide reinforced concrete composites containing recycled concrete aggregate, J. Build. Eng. 32 (2020) 101800.
[27] W. Long, D. Zheng, H. Duan, N. Han, F. Xing, Performance enhancement and environmental impact of cement composites containing graphene oxide with recycled fine aggregates, J. Clean. Prod. 194 (2018) 193–202.
[28] G. Fang, J. Chen, B. Dong, B. Liu, Microstructure and micromechanical properties of interfacial transition zone in green recycled aggregate concrete, J. Build. Eng. 66 (2023) 105860.
[29] L. Li, D. Xuan, A.O. Sojobi, S. Liu, S.H. Chu, C.S. Poon, Development of nano-silica treatment methods to enhance recycled aggregate concrete, Cem. Concr. Compos. 118 (2021) 103963.
[30] I. Gonzalez-Perez, J.L. Iserte, A. Fuentes, Implementation of Hertz theory and validation of a finite element model for stress analysis of gear drives with localized bearing contact, Mech. Mach. Theor. 46 (6) (2011) 765–783.
[31] L. Li, D. Xuan, A.O. Sojobi, S. Liu, S.H. Chu, C.S. Poon, Development of nano-silica treatment methods to enhance recycled aggregate concrete, Cem. Concr. Compos. 118 (2021) 103963.
[32] B.B. Mukharjee, S.V. Barai, Development of construction materials using nano-silica and aggregates recycled from construction and demolition waste, Waste Manag. Res. 33 (6) (2015) 515–523.
[33] J.F. Young, Looking ahead from the past: the heritage of cement chemistry, Cement Concr. Res. 38 (2) (2008) 111–114.
[34] S. Chiranjiakumari Devi, R. Ahmad Khan, Influence of graphene oxide on sulfate attack and carbonation of concrete containing recycled concrete aggregate, Construct. Build. Mater. 250 (2020) 118883.
[35] H. Yang, H. Cui, W. Tang, Z. Li, N. Han, F. Xing, A critical review on research progress of graphene/cement based composites, Compos. Part A-Appl. Sci. Manuf. 102 (2017) 273–296.
[36] L. Zhao, X. Guo, L. Song, Y. Song, G. Dai, J. Liu, An intensive review on the role of graphene oxide in cement-based materials, Construct. Build. Mater. 241 (2020) 117939.
[37] P. Zhan, J. Xu, J. Wang, C. Jiang, Multi-scale study on synergistic effect of cement replacement by metakaolin and typical supplementary cementitious materials on properties of ultra-high performance concrete, Construct. Build. Mater. 307 (2021) 125082.
[38] Z. He, P. Zhan, S. Du, B. Liu, W. Yuan, Creep behavior of concrete containing glass powder, Compos. B Eng. 166 (2019) 13–20.
[39] J. Zhang, T. Chen, X. Gao, Incorporation of self-ignited coal gangue in steam cured precast concrete, J. Clean. Prod. 292 (2021) 126004.
[40] W. Tian, Y. Liu, W. Wang, Multi-structural evolution of conductive reactive powder concrete manufactured by enhanced ohmic heating curing, Cem. Concr. Compos. 123 (2021) 104199.
[41] H. Huang, L. Teng, X. Gao, K.H. Khayat, F. Wang, Z. Liu, Effect of carbon nanotube and graphite nanoplatelet on composition, structure, and nano-mechanical properties of C-S-H in UHPC, Cem, Concr. Res. 154 (2022) 106713.
[42] W. Tian, M. Wang, Y. Liu, W. Wang, Ohmic heating curing of high content fly ash blended cement-based composites towards sustainable green construction materials used in severe cold region, J. Clean. Prod. 276 (2020) 123300.
[43] X.H. Wang, S. Jacobsen, J.Y. He, Z.L. Zhang, S.F. Lee, H.L. Lein, Application of nanoindentation testing to study of the interfacial transition zone in steel fiber reinforced mortar, Cement Concr. Res. 39 (8) (2009) 701–715.
[44] Y. Gao, G. De Schutter, G. Ye, Z. Tan, K. Wu, The ITZ microstructure, thickness and porosity in blended cementitious composite: effects of curing age, water to binder ratio and aggregate content, Compos. B Eng. 60 (2014) 1–13.
[45] W. Long, J. Wei, H. Ma, F. Xing, Dynamic mechanical properties and microstructure of graphene oxide nanosheets reinforced cement composites, Nanomaterials 7 (12) (2017) 407.
[46] J. Luo, S. Chen, Q. Li, C. Liu, S. Gao, J. Zhang, J. Guo, Influence of graphene oxide on the mechanical properties, fracture toughness, and microhardness of recycled concrete, Nanomaterials 9 (3) (2019) 325.
[47] A. Gladwin Alex, A. Kedir, T. Gebrehiwet Tewele, Review on effects of graphene oxide on mechanical and microstructure of cement-based materials, Construct. Build. Mater. 360 (2022) 129609.
[48] I.H. Alvi, Q. Li, Y. Hou, C.C. Onyekwena, M. Zhang, A. Ghaffar, A critical review of cement composites containing recycled aggregates with graphene oxide nanomaterials, J. Build. Eng. (2023) 105989.
[49] D. Lu, X. Shi, J. Zhong, Nano-engineering the interfacial transition zone in cement composites with graphene oxide, Construct. Build. Mater. 356 (2022) 129284.
[50] M.L. Berndt, Properties of sustainable concrete containing fly ash, slag and recycled concrete aggregate, Construct. Build. Mater. 23 (7) (2009) 2606–2613.

[51] J. Li, H. Xiao, Y. Zhou, Influence of coating recycled aggregate surface with pozzolanic powder on properties of recycled aggregate concrete, Construct. Build. Mater. 23 (3) (2009) 1287–1291.
[52] V.W.Y. Tam, C.M. Tam, K.N. Le, Removal of cement mortar remains from recycled aggregate using pre-soaking approaches, Resour. Conserv. Recycl. 50 (1) (2007) 82–101.
[53] D. Prasad, A. Pandey, B. Kumar, Sustainable production of recycled concrete aggregates by lime treatment and mechanical abrasion for M40 grade concrete, Construct. Build. Mater. 268 (2021) 121119.
[54] D. Xuan, B. Zhan, C.S. Poon, Development of a new generation of eco-friendly concrete blocks by accelerated mineral carbonation, J. Clean. Prod. 133 (2016) 1235–1241.
[55] C.-R. Wu, Y.-G. Zhu, X.-T. Zhang, S.-C. Kou, Improving the properties of recycled concrete aggregate with bio-deposition approach, Cem. Concr. Compos. 94 (2018) 248–254.
[56] C. Gao, L. Huang, L. Yan, R. Jin, H. Chen, Mechanical properties of recycled aggregate concrete modified by nano-particles, Construct. Build. Mater. 241 (2020) 118030.
[57] H. Chu, Y. Zhang, F. Wang, T. Feng, L. Wang, D. Wang, Effect of graphene oxide on mechanical properties and durability of ultra-high-performance concrete prepared from recycled sand, Nanomaterials 10 (9) (2020) 1718.
[58] L. Li, D. Xuan, S.H. Chu, J.X. Lu, C.S. Poon, Efficiency and mechanism of nano-silica pre-spraying treatment in performance enhancement of recycled aggregate concrete, Construct. Build. Mater. 301 (2021) 124093.
[59] H.-b. Hu, Z.-h. He, J.-y. Shi, C.-f. Liang, T.-g. Shibro, B.-j. Liu, S.-Y. Yang, Mechanical properties, drying shrinkage, and nano-scale characteristics of concrete prepared with zeolite powder pre-coated recycled aggregate, J. Clean. Prod. 319 (2021) 128710.
[60] C.-C. Chang, K.-C. Chang, W.-C. Lin, M.-H. Wu, Carbon footprint analysis in the aquaculture industry: assessment of an ecological shrimp farm, J. Clean. Prod. 168 (2017) 1101–1107.